

# Fluctuations and Pinning For Individually Manipulated Skyrmions

C. J. O. Reichhardt\* and C. Reichhardt

*Theoretical Division and Center for Nonlinear Studies, Los Alamos National Laboratory, Los Alamos, New Mexico 87545, USA*

Correspondence\*:  
C. J. O. Reichhardt  
cjr@lanl.gov

## ABSTRACT

We numerically examine the dynamics of individually dragged skyrmions interacting simultaneously with an array of other skyrmions and quenched disorder. For drives just above depinning, we observe a broad band noise signal with a  $1/f$  characteristic, while at higher drives, narrow band or white noise appears. Even in the absence of quenched disorder, the threshold force that must be applied to translate the driven skyrmion is finite due to elastic interactions with other skyrmions. The depinning threshold increases as the strength of the quenched disorder is raised. Above the depinning force, the skyrmion moves faster in the presence of quenched disorder than in a disorder-free system since the pinning sites prevent other skyrmions from being dragged along with the driven skyrmion. For strong pinning, we find a stick-slip motion of the driven skyrmion which produces a telegraph noise signature. The depinning threshold increases monotonically with skyrmion density in the absence of quenched disorder, but when pinning is present, the depinning threshold changes nonmonotonically with skyrmion density and there are reentrant pinned phases due to a competition between pinning induced by the quenched disorder and that produced by the elastic interactions of the skyrmion lattice.

**Keywords:** skyrmion, dynamic phases, broad band noise, telegraph noise, depinning

## 1 INTRODUCTION

Magnetic skyrmions in chiral magnets are particle-like textures that form a triangular lattice [Mühlbauer et al. (2009); Yu et al. (2010)] and can be set into motion under various types of drives [Nagaosa and Tokura (2013); Iwasaki et al. (2013); Schulz et al. (2012); Woo et al. (2016)]. Moving skyrmions can interact with each other as well as with impurities or quenched disorder in the sample [Nagaosa and Tokura (2013); Reichhardt et al. (2021)]. One consequence is the presence of a finite depinning threshold or critical driving force needed to set the skyrmions in motion. Depinning thresholds have been observed that span several orders of magnitude depending on the properties of the materials [Schulz et al. (2012); Woo et al. (2016); Reichhardt et al. (2021)]. Another interesting aspect of skyrmions is that their motion is strongly influenced by gyroscopic effects or the Magnus force. This force appears in addition to the dissipative effects that can arise from Gilbert damping and other sources. In the absence of quenched disorder, the Magnus force causes a driven skyrmion to move at a finite angle known as the skyrmion Hall angle  $\theta_{sk}$  with respect to the driving force, where the value of  $\theta_{sk}$  is proportional to the ratio of the Magnus to the damping forces [Nagaosa and Tokura (2013); Reichhardt et al. (2021); Everschor-Sitte and Sitte (2014); Reichhardt et al. (2015); Jiang et al. (2017); Litzius et al. (2017)]. When

quenched disorder is present,  $\theta_{sk}$  becomes velocity or drive dependent, starting from a zero value at low drives and gradually increasing with increasing velocity until it saturates at high drives to a value close to the intrinsic or disorder free Hall angle [Reichhardt et al. (2015); Jiang et al. (2017); Litzius et al. (2017); Reichhardt and Reichhardt (2019); Juge et al. (2019); Zeissler et al. (2020)]. Skyrmion depinning and motion can also be probed using the time series of the skyrmion velocity. Both numerical and experimental studies have shown that near the depinning transition, the skyrmion motion is disordered and the system exhibits large noise fluctuations with broad band or  $1/f^\alpha$  features, while at higher drives there is a crossover to white noise or even a narrow band or periodic noise signal [Díaz et al. (2017); Sato et al. (2019, 2020)]. The onset of narrow band noise is an indication that the skyrmions have formed a periodic lattice structure. Similar transitions between broad and narrow band noise as a function of drive have also been observed for the depinning and sliding dynamics of vortices in type-II superconductors [Marley et al. (1995); Olson et al. (1998)], driven charge density waves [Grüner (1988)], and other driven assemblies of particles moving over random quenched disorder [Reichhardt and Reichhardt (2017)].

Interest in skyrmion dynamics and pinning is driven in part by the prospect of using skyrmions in a variety of applications [Fert et al. (2017); Luo and You (2021)]. Many of these applications require the manipulation of individual skyrmions or the interaction of skyrmions with a disordered landscape, so understanding the motion and fluctuations of individually manipulated skyrmions would be a valuable step in this direction. There have been numerous studies of methods to manipulate or drag individual particles with and without quenched disorder which focused on the velocity and fluctuations of the manipulated particle. Examples include driving single colloids through assemblies of other colloids [Hastings et al. (2003); Habdas et al. (2004); Zia (2018); Dullens and Bechinger (2011); Gazuz et al. (2009)], as well as measuring the changes of the effective viscosity on the driven particle as the system goes through glass [Hastings et al. (2003); Habdas et al. (2004); Gazuz et al. (2009)], melting [Zia (2018); Dullens and Bechinger (2011)] or jamming transitions [Candelier and Dauchot (2010); Olson Reichhardt and Reichhardt (2010)]. Other studies have explored how the depinning threshold changes in a clean system as the system parameters are varied [Habdas et al. (2004); Olson Reichhardt and Reichhardt (2008); Gruber et al. (2020)], as well as the effect of quenched disorder on individually manipulated superconducting vortices and magnetic textures [Straver et al. (2008); Auslaender et al. (2009); Veshchunov et al. (2016); Kremen et al. (2016); Ma et al. (2018)]. It is also possible to examine changes in the fluctuations as a function of drive while the density of the surrounding medium or the coupling to quenched disorder is changed [Candelier and Dauchot (2010); Olson Reichhardt and Reichhardt (2010); Ma et al. (2018); Illien et al. (2018)]. In experiments on skyrmion systems, aspects of the pinning landscape have been examined by moving individual skyrmions with local tips [Hanneken et al. (2016); Holl et al. (2020)]. It is also possible to drag individual skyrmions with optical traps [Wang et al. (2020)] or by other means [Reichhardt and Reichhardt (2021)] and to examine the motion of the skyrmions within the traps as well as changes in the velocity and skyrmion Hall angle as function of driving force. Most of the extensive numerical and experimental studies of the dynamics of individually dragged particles have focused on bulk properties such as the average velocity or effective drag coefficients, and there is little work examining how the time series, noise fluctuations, or depinning threshold of a single probe particle would change when quenched disorder is present. This is of particular interest for skyrmions, since one could expect different fluctuations to appear in the damping dominated regime compared to the strong Magnus or gyroscopic dominated regime.

In this work we introduce quenched disorder to the system in order to expand on our previous study [Reichhardt and Reichhardt (2021)] of driving individual skyrmions through an assembly of other skyrmions. We specifically focus on the time series of the velocity fluctuations, noise power spectra,

effective drag, and changes in the depinning threshold while varying the ratio of the Magnus force to the damping. For strong damping, we generally find enhanced narrow band noise signals. We show that although quenched disorder can increase the depinning threshold, it can also decrease the drag experienced by the driven particle and reduce the amount of broad band noise. In the absence of quenched disorder, the depinning threshold monotonically increases with increasing system density [Reichhardt and Reichhardt (2021)], but we find that when quenched disorder is present, the depinning becomes strongly nonmonotonic due to the competition between the pinning from the quenched disorder and the pinning from elastic interactions with the surrounding medium. This can also be viewed as an interplay between pinning [Reichhardt and Reichhardt (2017)] and jamming [Reichhardt and Reichhardt (2014)] behaviors.

## 2 SIMULATION AND SYSTEM

We consider a modified Thiele equation [Thiele (1973); Lin et al. (2013); Brown et al. (2018)] or particle-based approach in which a single skyrmion is driven through a two-dimensional assembly of other skyrmions and a quenched disorder landscape. The initial skyrmion positions are obtained using simulated annealing, so that in the absence of quenched disorder, the skyrmions form a triangular lattice. The equation of motion of the driven skyrmion is given by

$$\alpha_d \mathbf{v}_i - \alpha_m \hat{\mathbf{z}} \times \mathbf{v}_i = \mathbf{F}_i^{ss} + \mathbf{F}_i^p + \mathbf{F}_i^D. \quad (1)$$

Here, the instantaneous velocity is  $\mathbf{v}_i = d\mathbf{r}_i/dt$ ,  $\mathbf{r}_i$  is the position of skyrmion  $i$ , and  $\alpha_d$  is the damping coefficient arising from dissipative processes. The gyroscopic or Magnus force, given by the second term on the left hand side, is of magnitude  $\alpha_m$  and causes the skyrmions to move in the direction perpendicular to the net applied force. The repulsive skyrmion interaction force has the form [Lin et al. (2013)]  $\mathbf{F}_i^{ss} = \sum_{j=1}^{N_s} K_1(r_{ij}) \hat{\mathbf{r}}_{ij}$ , where  $r_{ij} = |\mathbf{r}_i - \mathbf{r}_j|$ ,  $\hat{\mathbf{r}}_{ij} = (\mathbf{r}_i - \mathbf{r}_j)/r_{ij}$ , and  $K_1$  is the modified Bessel function which decays exponentially for large  $r$ . Within the system are  $N_p$  non-overlapping randomly placed pinning sites which are modeled as parabolic traps with a maximum range of  $r_p$  that produce a pinning force given by  $\mathbf{F}_i^p = \sum_{k=1}^{N_p} (F_p/r_p)(\mathbf{r}_i - \mathbf{r}_k^{(p)}) \Theta(r_p - |\mathbf{r}_i - \mathbf{r}_k^{(p)}|) \hat{\mathbf{r}}_{ik}^{(p)}$ , where  $F_p$  is the maximum pinning force and  $\Theta$  is the Heaviside step function. The driving force  $\mathbf{F}_i^D = F_D \hat{\mathbf{x}}$  is applied only to a single skyrmion. Under this driving force, in the absence of pinning or collisions with other skyrmions the skyrmion would move with an intrinsic skyrmion Hall angle of  $\theta_{sk}^{\text{int}} = \arctan(\alpha_m/\alpha_d)$ . We measure the net skyrmion velocity  $\mathbf{V} = N_s^{-1} \sum_{i=1}^{N_s} \mathbf{v}_i$  and its time-averaged components parallel,  $\langle V_{\parallel} \rangle$ , and perpendicular,  $\langle V_{\perp} \rangle$ , to the driving force, which is applied along the  $x$  direction. The measured skyrmion Hall angle is  $\theta_{sk} = \arctan(\langle V_{\perp} \rangle / \langle V_{\parallel} \rangle)$ . The sample is of size  $L \times L$  with  $L = 36$ , and in most of this work we consider  $N_s = 648$ , giving a skyrmion density of  $n_s = N_s/L^2 = 0.5$ , and  $N_p = 388$ , giving a pinning site density of  $n_p = N_p/L^2 = 0.3$ .

In previous work, we considered a similar model containing no pinning [Reichhardt and Reichhardt (2021)], where a finite critical depinning force  $F_c$  for motion of the driven skyrmion arises due to elastic interactions with the background skyrmions. There is also a higher second depinning force  $F_c^{\text{tr}}$  at which the driven skyrmion begins to move transverse to the driving direction, producing a finite skyrmion Hall angle.  $\theta_{sk}$  increases with increasing drive until, for high drives, it reaches a value close to the intrinsic value  $\theta_{sk}^{\text{int}}$ . This is similar to the behavior found for an assembly of skyrmions driven over random disorder [Reichhardt et al. (2015); Jiang et al. (2017); Litzius et al. (2017); Reichhardt and Reichhardt (2019); Juge et al. (2019); Zeissler et al. (2020); Díaz et al. (2017)]. For a fixed drive, the net velocity of the driven skyrmion can actually increase with increasing system density due to the Magnus-induced velocity

boost effect, whereas in the overdamped limit, the velocity decreases monotonically with increasing density due to enhanced damping from the increased frequency of collisions with background skyrmions [Reichhardt and Reichhardt (2021)]. In the present work, we study the effects of adding quenched disorder, and we measure time dependent velocity fluctuations, velocity overshoots, and the depinning threshold. The time series can be characterized by the power spectrum

$$S(\omega) = \left| \int V(t) \exp(-i\omega t) dt \right|^2 \quad (2)$$

Power spectra provide a variety of information on the dynamical properties of the system [Weissman (1988)] and have been used extensively to characterize depinning phenomena [Marley et al. (1995); Olson et al. (1998); Grüner (1988); Reichhardt and Reichhardt (2017); Bullard et al. (2008); Reichhardt and Reichhardt (2016)]. In this work we focus specifically on the fluctuations of the velocity component in the direction of drive.

### 3 RESULTS

In Fig. 1 we illustrate a subsection of the system containing a single skyrmion driven through a background of other skyrmions (blue dots) and pinning sites (open circles). The skyrmion trajectories indicate that the driven skyrmion creates a distortion in the surrounding medium as it moves through the system.

In Fig. 2(a) we plot the average velocity parallel to the drive,  $\langle V_{\parallel} \rangle$ , versus  $F_D$  for the system in Fig. 1 with  $n_s = 0.5$ ,  $\alpha_m = 0.1$ , and  $\alpha_d = 0.995$ . Here, we employ the constraint  $\alpha_d^2 + \alpha_m^2 = 1.0$  [Reichhardt and Reichhardt (2021)], and the intrinsic skyrmion Hall angle is  $\theta_{sk}^{\text{int}} = -5.74^\circ$ . In the absence of quenched disorder, where  $n_p = 0$ , a depinning threshold appears near  $F_c^{np} = 0.1$ . For  $0.1 < F_D \leq 1.0$ , the skyrmion is moving but, as indicated in Figs. 2(b) and (c),  $\langle V_{\perp} \rangle = 0$  and thus  $\theta_{sk} = 0^\circ$ . For  $F_D > 1.0$ ,  $\langle V_{\perp} \rangle$  becomes finite and  $\theta_{sk}$  begins to grow in magnitude with increasing  $F_D$  until it saturates near  $\theta_{sk} = -4.0^\circ$ . In a sample containing pinning with  $n_p = 0.3$  and  $F_p = 0.3$ , where the ratio of skyrmions to pinning sites is 5 : 3, the depinning threshold appears at  $F_c = 0.565$ . This value is higher than what would be observed in the single skyrmion limit, where  $F_c^{ss} = F_p = 0.3$ , indicating that the skyrmion-skyrmion interactions are playing an important role in the depinning process. It is also higher than the sum  $F_c^{ss} + F_c^{np} = 0.4$  of the single skyrmion and pin-free thresholds, showing that the skyrmions at the pinning sites produce an enhanced pinning effect on the driven skyrmion. In the sample with quenched disorder,  $\langle V_{\parallel} \rangle$  is finite for  $0.565 < F_D \leq 1.0$  but the corresponding  $\langle V_{\perp} \rangle = 0$ , while for  $F_D > 1.0$ , both  $\langle V_{\perp} \rangle$  and  $\theta_{sk}$  increase in magnitude with increasing  $F_D$ . In the regime  $F_D > 1.0$ ,  $\langle V_{\parallel} \rangle$  for the system containing pinning is higher than that found in the system without pinning. This is a result of the fact that in the clean system the driven skyrmion pushes some of the background skyrmions along with it, creating an enhanced drag which reduces  $\langle V_{\parallel} \rangle$ , whereas when pinning is present, the surrounding skyrmions are trapped by the pinning sites and cannot be entrained to move along with the driven skyrmion. The reverse trend appears in  $\langle V_{\perp} \rangle$ , where both the perpendicular velocity and the skyrmion Hall angle are smaller in magnitude when pinning is present than for the system without pinning.

In Fig. 3 we plot the depinning force  $F_c$  versus skyrmion density  $n_s$  for the systems in Fig. 2 with and without pinning. In the absence of pinning,  $F_c$  starts from zero and increases monotonically with increasing  $n_s$  as it becomes more difficult to push the skyrmion through the system. When pinning is present, at low  $n_s$  the driven skyrmion interacts only with the pinning sites, giving  $F_c = F_p$ ; however, once the density increases enough for the driven skyrmion to interact with both pinning sites and other skyrmions,  $F_c$  sharply increases and reaches a maximum value near  $n_s = 0.5$ . The maximum depinning

force  $F_c^{\max}$  should be approximately equal to the force needed to depin the driven skyrmion from a pinning site plus the force required to push the skyrmion directly in front of the driven skyrmion out of a pinning site,  $F_c^{\max} = 2F_p$ , which is close to the value we observe. Up to  $n_s = 0.5$ , the driven skyrmion can always find an empty pinning site to occupy. If the pinning were periodic, all pins would be filled once  $n_s = n_p$ , but since the pinning is randomly placed, some pins remain empty and available even when  $n_s$  is somewhat larger than  $n_p$ . Once  $n_s > 0.5$ ,  $F_c$  decreases with increasing  $n_s$  because the driven skyrmion is no longer able to find an available pinning site and is instead pinned only by the repulsion from the neighboring pinned skyrmions. This interstitial pinning is weaker than the direct pinning, and as  $n_s$  increases above  $n_s = 0.5$ , a larger and larger number of interstitial skyrmions appear in the sample, decreasing the fraction of directly pinned skyrmions and leading to the decrease in  $F_c$ . There are, however, still a nonzero fraction of pinned skyrmions, so  $F_c$  remains well above the value found in the sample without pinning sites. At large  $n_s$ ,  $F_c$  begins to increase with increasing density, in line with the trend found for the sample with no quenched pinning, where the interactions with an increasing number of unpinned skyrmions makes it more difficult for the driven skyrmion to move through the system. As  $n_s$  is increased beyond the range shown in Fig. 3, we expect that the curves for the pinned and unpinned samples will approach each other as the fraction of directly pinned skyrmions becomes smaller and smaller.

In Fig. 4(a) we plot the time series of the parallel velocity  $V_{\parallel}$  for the system in Fig. 2 at  $n_s = 0.5$  with no quenched disorder for  $F_D = 0.3$ , just above depinning. A series of short-period oscillations appear which correspond to elastic interactions in which the driven skyrmion moves past a background skyrmion without generating plastic displacements of the background skyrmions. There are also infrequent larger signals in the form of sharp velocity dips that are correlated with the creation of a plastic distortion or exchange of neighbors among the background skyrmions due to the passage of the driven skyrmion. In Fig. 4(b) we show the time series of  $V_{\parallel}$  for the system with quenched disorder at  $F_D = 0.625$ , just above the depinning threshold. Here, the motion is much more disordered, with strong short time velocity oscillations. These are produced by the motion of the driven skyrmion over the background pinning sites. The overall structure of the background skyrmions is disordered, destroying the periodic component of motion found in the unpinned system.

We next examine the power spectra  $S(\omega)$  of time series such as those shown in Fig. 4 for different drives for the systems in Fig. 2. Generically, power spectra can take several forms including  $1/f^\alpha$ , where  $\alpha = 0$  indicates white noise with little or no correlation,  $\alpha = 2$  is Brownian noise, and  $\alpha = 1$  or pink noise can appear when large scale collective events occur [Weissman (1988)]. Noise signatures that are periodic produce narrow band signals with peaks at specific frequencies. It is also possible to have combinations in which the signal is periodic on one time scale but has random fluctuations on longer time scales. For assemblies of particles under an applied drive that exhibit plastic depinning, the power spectrum is typically of  $1/f^\alpha$  type with  $\alpha$  ranging from  $\alpha = 1.3$  to  $\alpha = 2.0$ . A single particle moving over an uncorrelated random landscape typically shows a white noise spectrum, while motion over a periodic substrate produces narrow band noise features [Reichhardt and Reichhardt (2017)].

In Fig. 5(a) we plot  $S(\omega)$  for the disorder-free system with  $n_p = 0$  from Fig. 2 at  $F_D = 0.2$ , just above the depinning threshold. At low frequencies we find a series of oscillations or a narrow band noise feature. These periodic velocity oscillations correspond to the driven skyrmion speeding up and slowing down as it moves through the roughly triangular lattice formed by the surrounding skyrmions. The driven skyrmion occasionally generates dislocations or topological defects in the background lattice, so the motion is not strictly periodic but exhibits a combination of periodic motion with intermittent large bursts. This intermittent signal is what gives the spectrum an overall  $1/f^\alpha$  shape, as indicated by the red line which

is a fit with  $\alpha = 1.25$ . The noise power drops at higher frequencies, which are correlated with the small rotations caused by the Magnus force as the driven skyrmion generates plastic events. In Fig. 5(b) we show the velocity spectrum in the disorder-free sample at  $F_D = 0.3$  for the time series illustrated in Fig. 4(a). The overall shape of the spectrum is similar to that found at  $F_D = 0.2$  in Fig. 5(a), but the low frequency oscillations are reduced since more plastic events are occurring in the background skyrmion lattice. A power law fit with  $\alpha = 0.85$  appears as a straight line in Fig. 5(b). In overdamped driven systems with quenched disorder, the power law exponent is observed to decrease with increasing drive until it reaches a white noise state with  $\alpha = 0$ , and a narrow band noise signature appears at high drives [Marley et al. (1995); Olson et al. (1998); Reichhardt and Reichhardt (2017)]. In Fig. 5(c) at  $F_D = 1.0$ , the response at lower frequencies has become a white noise spectrum with  $\alpha = 0$ , while at slightly higher frequencies there is the beginning of a narrow band noise peak. At  $F_D = 1.5$  in Fig. 5(d), strong narrow band peaks appear in the spectrum. The narrow band noise arises once the driven skyrmion is moving fast enough that it no longer has time to generate dislocations or other defects in the surrounding lattice, making the system appear more like a single particle moving over a triangular lattice and creating few to no distortions. For high drives, the same narrow band noise signal appears but the peaks shift to higher frequencies as the driven skyrmion moves faster.

In Fig. 6(a) we plot  $S(\omega)$  for the pinned system with  $n_p = 0.3$  and  $F_p = 0.3$  from Fig. 4(b) at  $F_D = 0.625$ , just above depinning. At low frequencies, the power spectrum is nearly white with  $\alpha = 0$ , while the noise power drops as  $1/f^2$  at high frequencies. Unlike the pin-free system, strong low frequency oscillations are absent because the lattice structure of the surrounding skyrmions is disordered by the pinning sites. We find no  $1/f$  noise, in part due to the reduced mobility of the skyrmions trapped at pinning sites, which reduces the amount of plastic events which can occur. In the absence of pinning, the driven skyrmion can more readily create exchanges of neighbors in the background skyrmions, generating longer range distortions in the system and creating more correlated fluctuations in the driven skyrmion velocity. In Fig. 6(b) we plot  $S(\omega)$  for the same system at a higher drive of  $F_D = 1.5$ , where again similar white noise appears at low frequencies, while the transition from white noise to  $1/f^2$  noise has shifted to higher frequency. Unlike the disorder-free sample, here we find no narrow band signal since the surrounding skyrmions are trapped in disordered positions by the pinning. The addition of quenched disorder might be expected to increase the appearance of  $1/f$  noise due to the greater disorder in the system; however, in this case, the quenched disorder suppresses the plastic events responsible for the broad band noise signature. In a globally driven assembly of particles, the drive itself can induce plastic events [Reichhardt and Reichhardt (2017)]. This implies that the fluctuations of a single probe particle driven over quenched disorder are expected to differ significantly from the noise signatures found in bulk driven systems. The spectra in Fig. 6 have a shape called Lorentzian,  $S(f) = A/(\omega_0^2 + \omega^2)$ , which is also found for shot noise. [Weissman (1988)]. In our case,  $\omega_0$  corresponds to the average time between collisions of the driven skyrmion with pinning sites, and it shifts to higher frequencies as the drive increases.

We next consider the influence of the Magnus force on the noise fluctuations of the driven skyrmion. In Fig. 7(a) we plot the time series of  $V_{\parallel}$  at  $F_D = 1.0$  for a system without quenched disorder in the completely overdamped limit of  $\alpha_m = 0.0$  and  $\alpha_d = 1.0$ . For the equivalent drive in a sample with  $\alpha_m = 0.1$  and  $\alpha_d = 0.995$ , Fig. 5(c) shows that white noise is present; however, for the overdamped system, Fig. 7(b) indicates that a strong narrow band noise signal appears. In the image in Fig. 8(a), the driven skyrmion moves through the lattice of other skyrmions without creating plastic distortions. In general, we find that in the overdamped limit and in the absence of pinning, a strong narrow band noise signal appears as the driven skyrmion moves elastically through an ordered skyrmion lattice, as shown in the linear-linear plot of  $S(\omega)$  in Fig. 7(b). In Fig. 7(c) we plot the time series of  $V_{\parallel}$  for the same system

in the Magnus dominated regime with  $\alpha_m/\alpha_d = 9.95$  and  $\theta_{sk}^{\text{int}} = 84.26^\circ$ . Here, a combination of periodic motion and plastic events occur, producing the much smaller narrow band noise signal shown in Fig. 7(d). In the corresponding skyrmion trajectories illustrated in Fig. 8(b), the skyrmion moves at an angle to the driving direction due to the Magnus force, and there are significant distortions of the surrounding skyrmion lattice. This additional motion is generated by the increase in spiraling behavior produced by the Magnus force. In previous studies of bulk driven skyrmions moving over quenched disorder, it was shown that an increase in the Magnus force caused a reduction in the narrow band noise signal [Díaz et al. (2017)].

We next consider the effect of the pinning strength on the dynamics. In Fig. 9(a) we plot the time series of  $V_{\parallel}$  for a system with  $\alpha_m/\alpha_d = 0.1$ ,  $n_s = 0.5$ ,  $n_p = 0.3$ ,  $F_p = 2.0$ , and  $F_D = 1.6$ . Here the driven skyrmion experiences a combination of sliding and nearly pinned motion, where at certain points the skyrmion is temporarily trapped by a combination of the pinning and the skyrmion-skyrmion interactions. As the surrounding skyrmions relax, the driven skyrmion can jump out of the pinning site where it has become trapped, leading to another pulse of motion. This stick-slip or telegraph type motion only occurs just above the critical driving force when the pinning force is sufficiently strong, while for higher drives the motion becomes continuous. In Fig. 9(b) we show the time series of  $V_{\parallel}$  for the same system at  $\alpha_m/\alpha_d = 9.95$ , where the stick-slip or telegraph motion is lost. We note that the value of  $\langle V_{\parallel} \rangle$  in the Magnus dominated  $\alpha_m/\alpha_d = 9.95$  system is smaller than that found in the overdamped  $\alpha_m/\alpha_d = 0.1$  system since the increasing Magnus force rotates more of the velocity into the direction perpendicular to the drive; however, a similar continuous flow is observed both parallel and perpendicular to the drive in the Magnus dominated system. The loss of the stick-slip motion is due to the increasing spiraling motion of both the driven and background skyrmions. In Fig. 9(c) we plot the power spectra corresponding to the time series in Figs. 9(a,b). The stick-slip motion of the  $\alpha_m/\alpha_d = 0.1$  system produces a  $1/f^\alpha$  signature in  $S(\omega)$  with  $\alpha = 1.3$ . For the  $\alpha_m/\alpha_d = 9.95$  sample,  $S(\omega)$  is much flatter, indicating reduced correlations in the fluctuations, and also has increased noise power at high frequencies. The enhanced high frequency noise results from the fast spiraling motion of both the driven and the background skyrmions when they are inside pinning sites. The detection of enhanced high frequency noise could thus provide an indication that strong pinning effects or strong Magnus forces are present. In Fig. 9(d) we plot the distribution  $P(V_{\parallel})$  of instantaneous velocity for the samples in Figs. 9(a,b). When  $\alpha_m/\alpha_d = 0.1$ ,  $P(V_{\parallel})$  is bimodal with a large peak near  $V_{\parallel} = 0$  and a smaller peak near  $V = 1.6$ , corresponding to the value of the driving force. There is no gap of zero weight in  $P(V_{\parallel})$  separating these two peaks. When  $\alpha_m/\alpha_d = 9.95$ ,  $P(V_{\parallel})$  has only a single peak at intermediate velocities. Additionally, there is significant weight at negative velocities, which were not present in the strongly damped sample. The negative velocities arise when the skyrmions move in circular orbits due to the Magnus force and spend a portion of the orbit moving in the direction opposite to the driving force.

In Fig. 10(a) we plot the average velocity  $\langle V_{\parallel} \rangle$  versus pinning strength  $F_p$  for the system in Fig. 9(a) with  $\alpha_m/\alpha_d = 0.1$ ,  $n_s = 0.5$ , and  $n_p = 0.3$  at  $F_D = 2.0, 1.75, 1.5, 1.25, 1.0, 0.75$ , and  $0.5$ . The pinning force at which  $\langle V_{\parallel} \rangle$  reaches zero, indicating the formation of a pinned state, increases as  $F_D$  increases. Generally there is also a range of low  $F_p$  over which  $\langle V_{\parallel} \rangle$  increases with increasing  $F_p$ . This is due to a reduction in the drag on the driven skyrmion as the background skyrmions become more firmly trapped in the pinning sites, similar to what was illustrated in Fig. 2. Stick-slip motion appears in the regime where there is a sharp downturn in  $\langle V_{\parallel} \rangle$ , and is associated with a bimodal velocity distribution of the type shown in Fig. 9(d). A plot of  $\langle V_{\parallel} \rangle$  versus  $F_p$  for the  $\alpha_m/\alpha_d = 9.95$  system (not shown) reveals a similar trend, except that the pinning transitions shift to larger values of  $F_p$ . Using the features in Fig. 10(a) combined

with the velocity distributions, we construct a dynamic phase diagram for the  $\alpha_m/\alpha_d = 0.1$  system as a function of  $F_p$  versus  $F_D$ , illustrated in Fig. 10(b). We observe continuous flow, stick slip motion, and pinned regimes, with stick-slip motion occurring only when  $F_p > 0.75$ . In general, for increasing Magnus force, the window of stick-slip motion decreases in size.

In Fig. 11(a) we plot  $\langle V_{||} \rangle$  versus the skyrmion density  $n_s$  for the system in Fig. 9(a) with  $F_p = 1.6$ ,  $n_p = 0.3$ , and  $\alpha_m/\alpha_d = 0.1$  at  $F_D = 1.4, 1.6, 1.8, 2.0, 2.2, 2.4$ , and  $2.6$ . At  $F_D = 1.4$  the system is pinned when  $n_s \leq 1.0$ . For this skyrmion density, all of the skyrmions can be trapped at pinning sites and are therefore unable to move since  $F_D < F_p$ . As  $n_s$  increases, all of the pinning sites become filled and interstitial skyrmions appear which are pinned only by repulsion from other skyrmions directly located at pinning sites. The strength of this interstitial pinning is determined by the elastic properties of the skyrmion lattice, and for these densities it is weaker than  $F_p$ . When  $F_D > F_p$ , flow can occur even for low  $n_s$ , where the driven skyrmion interacts with the pinning sites but has few collisions with background skyrmions. In the limit  $n_s = 0$  where only the driven skyrmion is present, the system is always flowing whenever  $F_D/F_p > 1.0$ . For the  $F_D = 2.2$  curve, the system is flowing up to  $n_s = 0.2$  and then a pinned region appears for  $0.2 < n_s < 0.5$ . At this range of skyrmion densities, even though  $F_D > F_p$ , the driven skyrmion experiences a combination of direct pinning from the pinning sites it encounters plus interstitial pinning by the nearby directly pinned skyrmions, giving an additive effect which causes the apparent pinning strength to be larger than  $F_D$ . For  $n_s > 0.5$ , all the pinning sites start to become occupied and the driven skyrmion experiences only the weaker interstitial pinning without becoming trapped directly by any pinning sites. At small  $F_D$  it is possible for the driven skyrmion to become trapped by a pinning site that is already occupied by a background skyrmion, creating a doubly occupied pinning site, which is why the value of  $n_s$  below which the driven skyrmion can begin to move again shifts to larger  $n_s$  with decreasing  $F_D$ . The reentrant pinning effect illustrated in Fig. 11(a) arises from the combination of the direct and interstitial pinning mechanisms. In Fig. 11(b) we construct a dynamic phase diagram as a function of  $n_s/n_p$  versus  $F_D$  for the system in Fig. 11(a) showing the pinned and flowing phases. Reentrant pinning occurs over the range  $F_D = F_p = 1.6$  to slightly above  $F_D = 2.2$ . The reentrant pinned phase reaches its maximum extent near  $n_s/n_p = 1.0$ , a density at which the number of directly pinned skyrmions attains its maximum value while the number of interstitially pinned skyrmions is still nearly zero.

For higher values of  $n_s/n_p$ , another pinned phase arises at low values of  $F_D$  that is produced by the skyrmion-skyrmion interactions. In Fig. 12(b) we plot  $\langle V_{||} \rangle$  versus  $n_s$  up to  $n_s = 4.0$  for  $F_D = 0.5, 0.75, 1.0, 1.2, 1.4$ , and  $1.6$  in the same system from Fig. 11. At higher  $n_s$ ,  $\langle V_{||} \rangle$  drops to zero again as the system reaches a pinned state. This second pinned phase is produced by the increase in the elastic skyrmion-skyrmion interaction energies at the higher densities. In the absence of quenched disorder, the skyrmion-skyrmion interactions are the only mechanism by which the driven skyrmion can be pinned, and there is a threshold for motion which increases monotonically with increasing  $n_s$ . When quenched disorder is introduced, the threshold becomes both non-monotonic and reentrant. For increasing  $F_D$  in Fig. 12(a), the elastic energy-induced pinning transition shifts to higher  $n_s$ . In Fig. 12(b) we show a dynamic phase diagram as a function of  $n_s/n_p$  versus  $F_D$  for the system in Fig. 12(a) indicating the locations of the pinned and flowing phases. For  $n_s/n_p < 2.0$ , the reentrant pinned state produced by a combination of direct and interstitial pinning reaches its maximum extent. As  $n_s/n_p$  increases, the pinned state reaches a minimum width near  $n_s/n_p = 5.5$ , above which the pinned region begins to grow again. The yellow dashed line is the depinning threshold in the absence of quenched disorder, which always falls below the depinning transition of samples with quenched disorder. The increase in the depinning threshold due to the addition of pinning occurs even when the number of skyrmions is significantly larger than the



number of pinning sites since even a relatively small number of pins can prevent plastic distortions of the background skyrmions, raising the barrier for motion of the driven skyrmion.

In the phase diagrams of Fig. 11(b) and Fig. 12(b), for drives just above the pinned phase, there is a small window of stick-slip motion (not shown) which is more prominent for lower values of  $n_s/n_p$ . In addition, within the flowing phase there is another critical drive above which there is an onset of transverse motion, giving a finite Hall angle. This line has a shape similar to that of the depinning curve but falls at higher values of  $F_D$ .

In this work we considered a point-like model for skyrmions. In real skyrmion systems, there is an effective skyrmion size that can change with field or exhibit internal modes. It may be possible that at low fields, the particle picture works well, while at higher fields, the skyrmions will start to change shape. It would be interesting to study how the effective drag on the driven skyrmion would change in this case. Another question regards the distinction between pinning-dominated pinned states, where direct pinning is responsible for producing the pinning, and interstitial-dominated or jammed pinned states, where the pinning of the driven skyrmion arises from elastic interactions with directly pinned skyrmions. The fluctuations in the jammed state generally show that there is a greater tendency for large scale plastic events to occur, leading to a larger amount of low frequency noise compared to the pinning-dominated state. In work on superconducting vortices with quenched disorder, the presence of pinned, jammed, and clogged phases could be deduced by measuring memory effects [Reichhardt and Reichhardt (2020)]. For the single driven skyrmion, memory could be tested by reversing the driving direction. For strong pinning, the trajectory under reversed drive should mirror that of the forward drive, indicating a memory effect, whereas in samples with strong plastic distortions, the trajectory for forward and reversed drive will differ due to the appearance of plastic distortions in the background skyrmions.

## 4 SUMMARY

We have examined the fluctuations and pinning effects for individually driven skyrmions moving through an assembly of other skyrmions and quenched disorder. We find that in the absence of quenched disorder, there is a depinning force which increases monotonically with increasing skyrmion density. When quenched disorder is introduced, the driven skyrmion experiences a combination of pinning and drag effects from both the pinning sites and the background skyrmions. Both with and without quenched disorder, there is a second, higher driving threshold for the onset of motion transverse to the drive and the appearance of a finite skyrmion Hall angle. For higher drives, addition of quenched disorder actually increases the velocity of the driven skyrmion since the pinning sites help prevent the background skyrmions from being dragged along by the driven skyrmion. Near depinning, in the absence of quenched disorder the velocity fluctuations show a combination of periodic oscillations from the elasticity of the ordered background skyrmion lattice along with stronger jumps associated with plastic distortions of the background skyrmions. This produces a velocity power spectrum that has narrow band noise peaks superimposed on a  $1/f^\alpha$  shape with  $\alpha = 1.2$ . As the drive increases, the spectrum becomes white, and for very high drives, a strong narrow band signature emerges once the driven skyrmion is moving too rapidly to generate plastic distortions in the background skyrmions. Addition of quenched disorder reduces the frequency of plastic events, giving a white noise spectrum. In the absence of disorder, a damping-dominated system generally shows strong narrow band noise fluctuations as the driven skyrmion moves along one-dimensional paths in the background skyrmion lattice, whereas in the Magnus-dominated limit, the driven skyrmion moves at an angle through the lattice, generating dislocations and reducing the strength of the narrow band signature. When the disorder is strong, the driven skyrmion can undergo stick-slip motion due to a combination of being trapped at pinning sites and interacting elastically with

the background skyrmions, which produces a bimodal velocity distribution along with  $1/f^\alpha$  noise. For systems with quenched disorder, the depinning threshold is highly non-monotonic as a function of the skyrmion density, passing through both peaks and minima. This is due to a competition between two different pinning effects. The depinning threshold drops when the number of skyrmions becomes larger than the number of pinning sites since the driven skyrmion must be pinned through interstitial interactions with directly pinned skyrmions instead of sitting in a pinning site directly; however, at higher densities, the increasing strength of the elastic interactions between the skyrmions causes the depinning threshold to rise again with increasing density. At low densities the system can be viewed as being in a pinning-dominated regime, while at higher densities it is in an interstitial-dominated or jamming regime. Beyond skyrmions, our results should be relevant to fluctuations in other particle-based systems such as individually dragged vortices in type-II superconductors.

## CONFLICT OF INTEREST STATEMENT

The authors declare that the research was conducted in the absence of any commercial or financial relationships that could be construed as a potential conflict of interest.

## AUTHOR CONTRIBUTIONS

All authors contributed equally to all portions of this work.

## FUNDING

We gratefully acknowledge the support of the U.S. Department of Energy through the LANL/LDRD program for this work. This work was supported by the US Department of Energy through the Los Alamos National Laboratory. Los Alamos National Laboratory is operated by Triad National Security, LLC, for the National Nuclear Security Administration of the U. S. Department of Energy (Contract No. 892333218NCA000001).

## REFERENCES

- Auslaender, O. M., Luan, L., Straver, E. W. J., Hoffman, J. E., Koshnick, N. C., Zeldov, E., et al. (2009). Mechanics of individual isolated vortices in a cuprate superconductor. *Nature Phys.* 5, 35–39. doi:10.1038/NPHYS1127
- Brown, B. L., Täuber, U. C., and Pleimling, M. (2018). Effect of the Magnus force on skyrmion relaxation dynamics. *Phys. Rev. B* 97, 020405. doi:10.1103/PhysRevB.97.020405
- Bullard, T. J., Das, J., Daquila, G. L., and Tauber, U. C. (2008). Vortex washboard voltage noise in type-II superconductors. *Eur. Phys. J. B* 65, 469–484. doi:10.1140/epjb/e2008-00358-7
- Candelier, R. and Dauchot, O. (2010). Journey of an intruder through the fluidization and jamming transitions of a dense granular media. *Phys. Rev. E* 81, 011304. doi:10.1103/PhysRevE.81.011304
- Díaz, S. A., Reichhardt, C. J. O., Arovas, D. P., Saxena, A., and Reichhardt, C. (2017). Fluctuations and noise signatures of driven magnetic skyrmions. *Phys. Rev. B* 96, 085106. doi:10.1103/PhysRevB.96.085106
- Dullens, R. P. A. and Bechinger, C. (2011). Shear thinning and local melting of colloidal crystals. *Phys. Rev. Lett.* 107, 138301. doi:10.1103/PhysRevLett.107.138301
- Everschor-Sitte, K. and Sitte, M. (2014). Real-space Berry phases: Skyrmion soccer (invited). *J. Appl. Phys.* 115, 172602. doi:10.1063/1.4870695
- Fert, A., Reyren, N., and Cros, V. (2017). Magnetic skyrmions: advances in physics and potential applications. *Nature Rev. Mater.* 2, 17031. doi:10.1038/natrevmats.2017.31

- Gazuz, I., Puertas, A. M., Voigtmann, T., and Fuchs, M. (2009). Active and nonlinear microrheology in dense colloidal suspensions. *Phys. Rev. Lett.* 102, 248302. doi:10.1103/PhysRevLett.102.248302
- Gruber, M., Puertas, A. M., and Fuchs, M. (2020). Critical force in active microrheology. *Phys. Rev. E* 101, 012612. doi:10.1103/PhysRevE.101.012612
- Grüner, G. (1988). The dynamics of charge-density waves. *Rev. Mod. Phys.* 60, 1129–1181. doi:10.1103/RevModPhys.60.1129
- Habdas, P., Schaar, D., Levitt, A. C., and Weeks, E. R. (2004). Forced motion of a probe particle near the colloidal glass transition. *Europhys. Lett.* 67, 477–483. doi:10.1209/epl/i2004-10075-y
- Hanneken, C., Kubetzka, A., von Bergmann, K., and Wiesendanger, R. (2016). Pinning and movement of individual nanoscale magnetic skyrmions via defects. *New J. Phys.* 18, 055009. doi:10.1088/1367-2630/18/5/055009
- Hastings, M. B., Olson Reichhardt, C. J., and Reichhardt, C. (2003). Depinning by fracture in a glassy background. *Phys. Rev. Lett.* 90, 098302. doi:10.1103/PhysRevLett.90.098302
- Holl, C., Knol, M., Pratzner, M., Chico, J., Fernandes, I. L., Lounis, S., et al. (2020). Probing the pinning strength of magnetic vortex cores with sub-nanometer resolution. *Nature Commun.* 11, 2833. doi:10.1038/s41467-020-16701-y
- Illien, P., Bénichou, O., Oshanin, G., Sarracino, A., and Voituriez, R. (2018). Nonequilibrium fluctuations and enhanced diffusion of a driven particle in a dense environment. *Phys. Rev. Lett.* 120, 200606. doi:10.1103/PhysRevLett.120.200606
- Iwasaki, J., Mochizuki, M., and Nagaosa, N. (2013). Universal current-velocity relation of skyrmion motion in chiral magnets. *Nature Commun.* 4, 1463. doi:10.1038/ncomms2442
- Jiang, W., Zhang, X., Yu, G., Zhang, W., Wang, X., Jungfleisch, M. B., et al. (2017). Direct observation of the skyrmion Hall effect. *Nature Phys.* 13, 162–169. doi:10.1038/NPHYS3883
- Juge, R., Je, S.-G., Chaves, D. d. S., Buda-Prejbeanu, L. D., Peña Garcia, J., Nath, J., et al. (2019). Current-driven skyrmion dynamics and drive-dependent skyrmion Hall effect in an ultrathin film. *Phys. Rev. Applied* 12, 044007. doi:10.1103/PhysRevApplied.12.044007
- Kremen, A., Wissberg, S., Haham, N., Persky, E., Frenkel, Y., and Kalisky, B. (2016). Mechanical control of individual superconducting vortices. *Nano Lett.* 16, 1626–1630. doi:10.1021/acs.nanolett.5b04444
- Lin, S.-Z., Reichhardt, C., Batista, C. D., and Saxena, A. (2013). Particle model for skyrmions in metallic chiral magnets: Dynamics, pinning, and creep. *Phys. Rev. B* 87, 214419. doi:10.1103/PhysRevB.87.214419
- Litzius, K., Lemesh, I., Krüger, B., Bassirian, P., Caretta, L., Richter, K., et al. (2017). Skyrmion Hall effect revealed by direct time-resolved X-ray microscopy. *Nature Phys.* 13, 170–175. doi:10.1038/NPHYS4000
- Luo, S. and You, L. (2021). Skyrmion devices for memory and logic applications. *APL Materials* 9, 050901. doi:10.1063/5.0042917
- Ma, X., Reichhardt, C. J. O., and Reichhardt, C. (2018). Manipulation of individual superconducting vortices and stick-slip motion in periodic pinning arrays. *Phys. Rev. B* 97, 214521. doi:10.1103/PhysRevB.97.214521
- Marley, A. C., Higgins, M. J., and Bhattacharya, S. (1995). Flux flow noise and dynamical transitions in a flux line lattice. *Phys. Rev. Lett.* 74, 3029–3032. doi:10.1103/PhysRevLett.74.3029
- Mühlbauer, S., Binz, B., Jonietz, F., Pfleiderer, C., Rosch, A., Neubauer, A., et al. (2009). Skyrmion lattice in a chiral magnet. *Science* 323, 915–919. doi:10.1126/science.1166767
- Nagaosa, N. and Tokura, Y. (2013). Topological properties and dynamics of magnetic skyrmions. *Nature Nanotechnol.* 8, 899–911. doi:10.1038/NNANO.2013.243

- Olson, C. J., Reichhardt, C., and Nori, F. (1998). Nonequilibrium dynamic phase diagram for vortex lattices. *Phys. Rev. Lett.* 81, 3757–3760. doi:10.1103/PhysRevLett.81.3757
- Olson Reichhardt, C. J. and Reichhardt, C. (2008). Viscous decoupling transitions for individually dragged particles in systems with quenched disorder. *Phys. Rev. E* 78, 011402. doi:10.1103/PhysRevE.78.011402
- Olson Reichhardt, C. J. and Reichhardt, C. (2010). Fluctuations, jamming, and yielding for a driven probe particle in disordered disk assemblies. *Phys. Rev. E* 82, 051306. doi:10.1103/PhysRevE.82.051306
- Reichhardt, C., Ray, D., and Reichhardt, C. J. O. (2015). Collective transport properties of driven skyrmions with random disorder. *Phys. Rev. Lett.* 114, 217202. doi:10.1103/PhysRevLett.114.217202
- Reichhardt, C. and Reichhardt, C. J. O. (2014). Aspects of jamming in two-dimensional athermal frictionless systems. *Soft Matter* 10, 2932–2944. doi:10.1039/c3sm53154f
- Reichhardt, C. and Reichhardt, C. J. O. (2016). Noise fluctuations and drive dependence of the skyrmion Hall effect in disordered systems. *New J. Phys.* 18, 095005. doi:10.1088/1367-2630/18/9/095005
- Reichhardt, C. and Reichhardt, C. J. O. (2017). Depinning and nonequilibrium dynamic phases of particle assemblies driven over random and ordered substrates: a review. *Rep. Prog. Phys.* 80, 026501. doi:10.1088/1361-6633/80/2/026501
- Reichhardt, C. and Reichhardt, C. J. O. (2019). Thermal creep and the skyrmion Hall angle in driven skyrmion crystals. *J. Phys.: Condens. Matter* 31, 07LT01. doi:10.1088/1361-648X/aaefd7
- Reichhardt, C. and Reichhardt, C. J. O. (2020). Jamming, fragility and pinning phenomena in superconducting vortex systems. *Sci. Rep.* 10, 11625. doi:10.1038/s41598-020-68417-0
- Reichhardt, C. and Reichhardt, C. J. O. (2021). Dynamics and nonmonotonic drag for individually driven skyrmions. *Phys. Rev. B* 104, 064441. doi:10.1103/PhysRevB.104.064441
- Reichhardt, C., Reichhardt, C. J. O., and Milosevic, M. V. (2021). Statics and dynamics of skyrmions interacting with pinning: a review. *arXiv e-prints*, arXiv:2102.10464
- Sato, T., Kikkawa, A., Taguchi, Y., Tokura, Y., and Kagawa, F. (2020). Mode locking phenomena of the current-induced skyrmion-lattice motion in microfabricated MnSi. *Phys. Rev. B* 102, 180411. doi:10.1103/PhysRevB.102.180411
- Sato, T., Koshibae, W., Kikkawa, A., Yokouchi, T., Oike, H., Taguchi, Y., et al. (2019). Slow steady flow of a skyrmion lattice in a confined geometry probed by narrow-band resistance noise. *Phys. Rev. B* 100, 094410. doi:10.1103/PhysRevB.100.094410
- Schulz, T., Ritz, R., Bauer, A., Halder, M., Wagner, M., Franz, C., et al. (2012). Emergent electrodynamics of skyrmions in a chiral magnet. *Nature Phys.* 8, 301–304. doi:10.1038/NPHYS2231
- Straver, E. W. J., Hoffman, J. E., Auslaender, O. M., Rugar, D., and Moler, K. A. (2008). Controlled manipulation of individual vortices in a superconductor. *Appl. Phys. Lett.* 93, 172514. doi:10.1063/1.3000963
- Thiele, A. A. (1973). Steady-state motion of magnetic domains. *Phys. Rev. Lett.* 30, 230–233. doi:10.1103/PhysRevLett.30.230
- Veshchunov, I. S., Magrini, W., Mironov, S. V., Godin, A. G., Trebbia, J. B., Buzdin, A. I., et al. (2016). Optical manipulation of single flux quanta. *Nature Commun.* 7, 12801. doi:10.1038/ncomms12801
- Wang, X.-G., Chotorlishvili, L., Dugaev, V. K., Ernst, A., Maznichenko, I. V., Arnold, N., et al. (2020). The optical tweezer of skyrmions. *npj Comput. Mater.* 6, 140. doi:10.1038/s41524-020-00402-7
- Weissman, M. B. (1988).  $\frac{1}{f}$  noise and other slow, nonexponential kinetics in condensed matter. *Rev. Mod. Phys.* 60, 537–571. doi:10.1103/RevModPhys.60.537
- Woo, S., Litzius, K., Krüger, B., Im, M.-Y., Caretta, L., Richter, K., et al. (2016). Observation of room-temperature magnetic skyrmions and their current-driven dynamics in ultrathin metallic ferromagnets.

*Nature Mater.* 15, 501. doi:10.1038/NMAT4593

Yu, X. Z., Onose, Y., Kanazawa, N., Park, J. H., Han, J. H., Matsui, Y., et al. (2010). Real-space observation of a two-dimensional skyrmion crystal. *Nature (London)* 465, 901–904. doi:10.1038/nature09124

Zeissler, K., Finizio, S., Barton, C., Huxtable, A. J., Massey, J., Raabe, J., et al. (2020). Diameter-independent skyrmion Hall angle observed in chiral magnetic multilayers. *Nature Commun.* 11, 428. doi:10.1038/s41467-019-14232-9

Zia, R. N. (2018). Active and passive microrheology: Theory and simulation. *Ann. Rev. Fluid Mech.* 50, 371. doi:10.1146/annurev-fluid-122316-044514

## FIGURE CAPTIONS

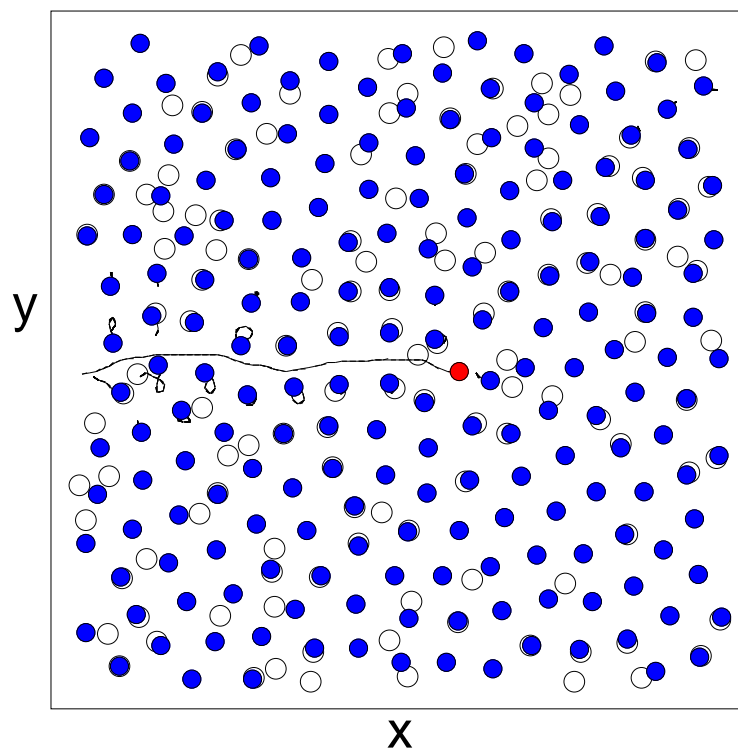


**Figure 1.** An image of a subsection of the system in which a single skyrmion (red) is driven through an assembly of other skyrmions (blue) in the presence of quenched disorder, generated by randomly placed nonoverlapping local trapping sites (open circles). Black lines indicate the skyrmion trajectories. The driven skyrmion generates motion of the surrounding skyrmions as it passes through the system.

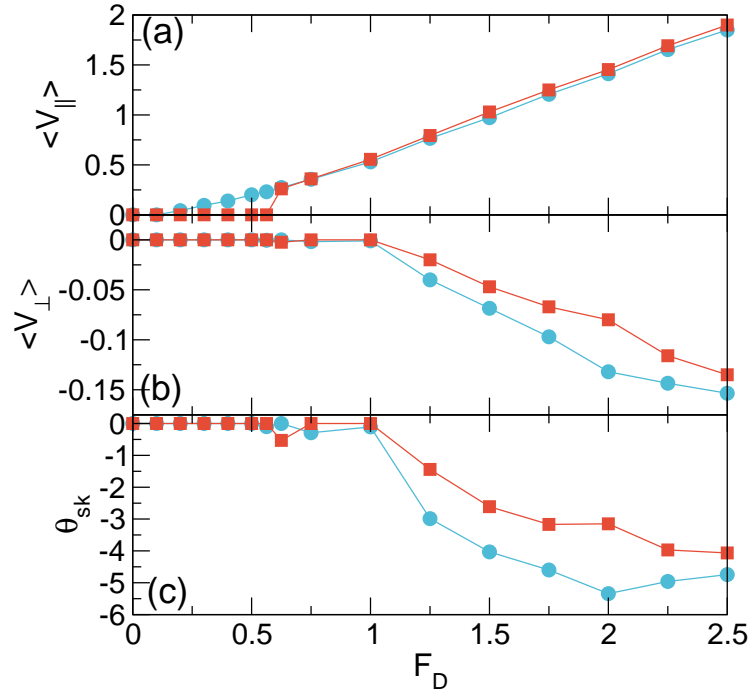


**Figure 2.** a) The velocity  $\langle V_{\parallel} \rangle$  parallel to the driving direction versus drive  $F_D$  for the system in Fig. 1 with  $n_s = 0.5$ ,  $\alpha_m = 0.1$ ,  $\alpha_d = 0.995$ , and  $\theta_{sk}^{\text{int}} = -5.74^\circ$ . Blue circles are for a system with no pinning,  $n_p = 0$ , while red squares are for a system with  $n_p = 0.3$  and  $F_p = 0.3$ . (b) The corresponding velocity in the perpendicular direction  $\langle V_{\perp} \rangle$  versus  $F_D$ . (c) The corresponding measured skyrmion Hall angle  $\theta_{sk}$  versus  $F_D$ .

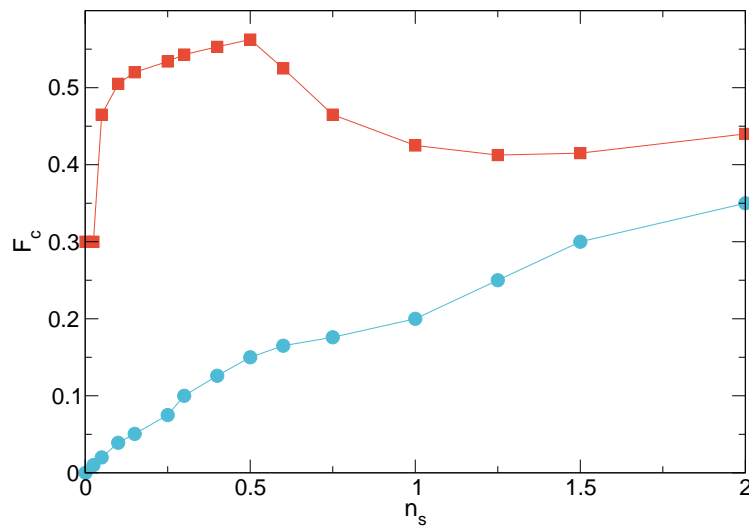


**Figure 3.** The depinning force  $F_c$  versus skyrmion density  $n_s$  for the systems in Fig. 2 with  $\alpha_m = 0.1$ ,  $\alpha_d = 0.995$ , and  $\theta_{sk}^{\text{int}} = -5.74^\circ$ . Blue circles are for a pin-free system with  $n_p = 0$  while red squares are for a system with  $n_p = 0.3$  and  $F_p = 0.3$ . With no quenched disorder,  $F_c$  increases monotonically with  $n_s$ .

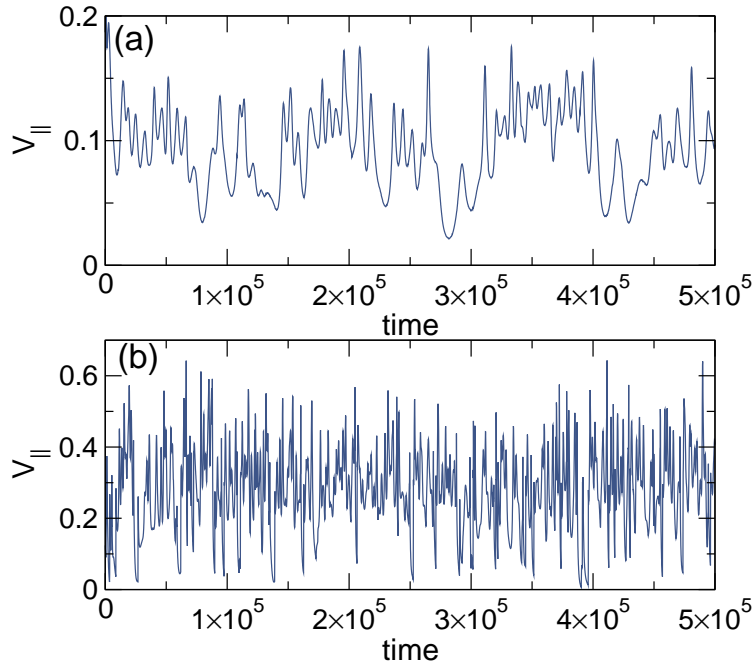


**Figure 4.** The time series of the velocity  $V_{\parallel}$  parallel to the drive for the system in Fig. 2 with  $n_s = 0.5$ ,  $\alpha_m = 0.1$ ,  $\alpha_d = 0.995$ , and  $\theta_{sk}^{int} = -5.74^\circ$ . (a) The disorder-free  $n_p = 0$  system at  $F_D = 0.3$  just above depinning, showing periodic oscillations and longer time plastic events. (b) The quenched disorder system with  $n_p = 0.3$  and  $F_p = 0.3$  at  $F_D = 0.625$  just above depinning, showing less correlated motion.

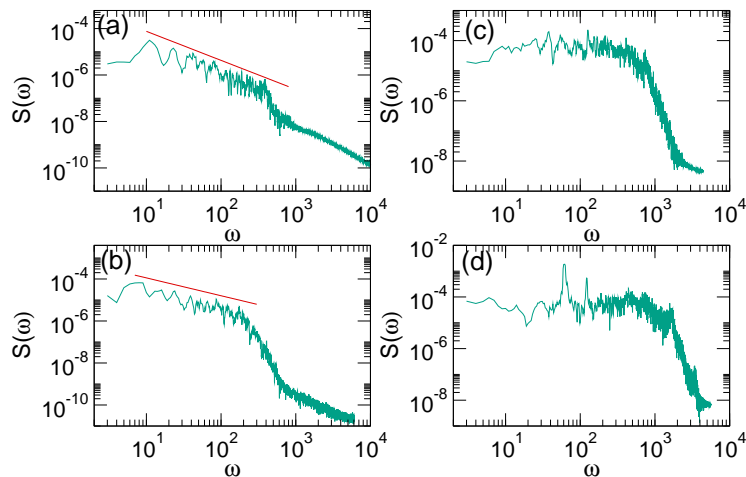


**Figure 5.** (a) The power spectra  $S(\omega)$  for the system in Fig. 2 with  $n_s = 0.5$ ,  $\alpha_m = 0.1$ ,  $\alpha_d = 0.995$ ,  $\theta_{sk}^{int} = -5.74^\circ$ , and no quenched disorder ( $n_p = 0$ ). (a) At  $F_D = 0.2$  there is a  $1/f^\alpha$  signature, where the straight line indicates  $\alpha = 1.25$ , along with a series of peaks corresponding to the oscillatory portion of the motion due to the periodicity of the skyrmion lattice. (b) At  $F_D = 0.3$ , the red line indicates  $\alpha = 0.85$ . (c) At  $F_D = 1.0$  the signal is white noise with  $\alpha = 0$ . (d) At  $F_D = 1.5$  there is a narrow band noise signal.

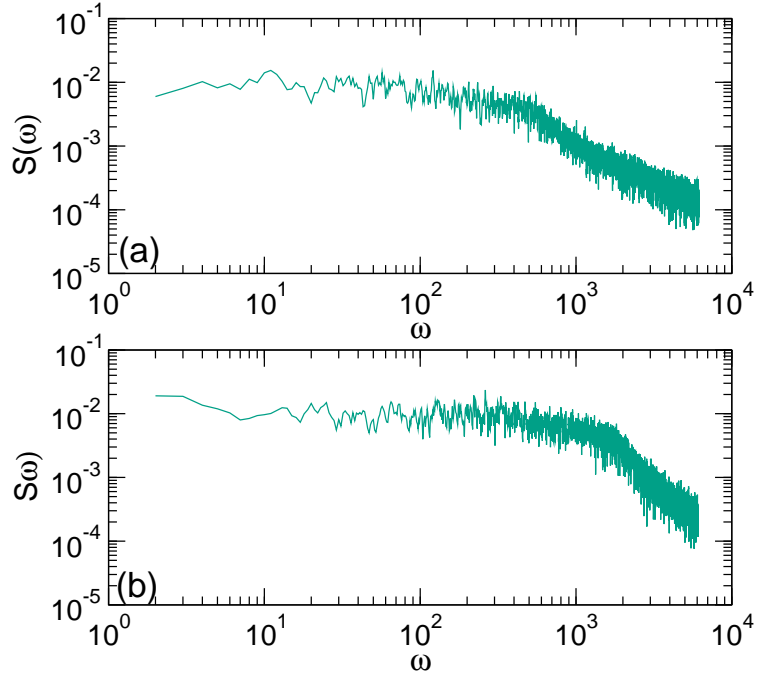


**Figure 6.** The power spectra  $S(\omega)$  for the system in Fig. 2 with quenched disorder at  $n_s = 0.5$ ,  $\alpha_m = 0.1$ ,  $\alpha_d = 0.995$ ,  $\theta_{sk}^{\text{int}} = -5.74^\circ$ ,  $n_p = 0.3$ , and  $F_p = 0.3$ . (a) At  $F_D = 0.625$ , the noise signal is close to white with  $\alpha = 0$ . (b) A similar spectrum appears at  $F_D = 1.5$ . The high frequency shoulder above which a  $1/f^2$  signature appears shifts to higher drives as  $F_D$  increases.

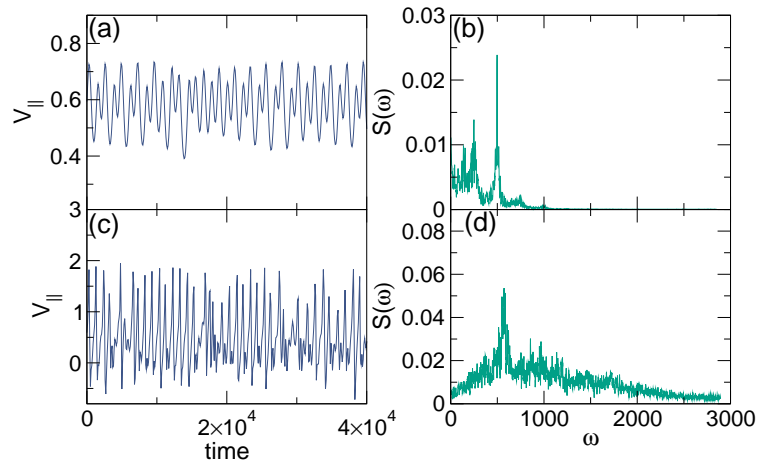


**Figure 7.** (a) The time series of the velocity  $V_{\parallel}$  parallel to the drive at  $n_s = 0.5$  and  $F_D = 1.0$  for an overdamped system with  $\alpha_m/\alpha_d = 0$  and no quenched disorder. (b) The corresponding power spectrum  $S(\omega)$  contains narrow band peaks. (c) The time series for the same system but with  $\alpha_m/\alpha_d = 9.95$ , where the fluctuations are enhanced. (d) The corresponding power spectrum  $S(\omega)$  has a reduced amount of narrow band noise.



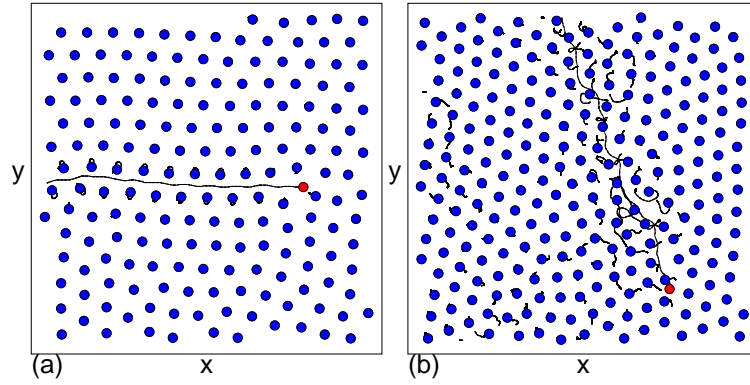


**Figure 8.** An image of a subsection of the system showing the driven skyrmion (red), background skyrmions (blue), and skyrmion trajectories (black lines) for the samples from Fig. 7 with  $n_s = 0.5$  at  $F_D = 1.0$ . (a) For the overdamped system with  $\alpha_m/\alpha_d = 0$  from Fig. 7(a,b), the background skyrmions experience elastic distortions but there are no plastic events. (b) For the Magnus dominated system with  $\alpha_m/\alpha_d = 9.95$  from Fig. 7(c,d), the driven skyrmion moves at an angle due to the increased Magnus force, creating significant distortions in the background skyrmion lattice.

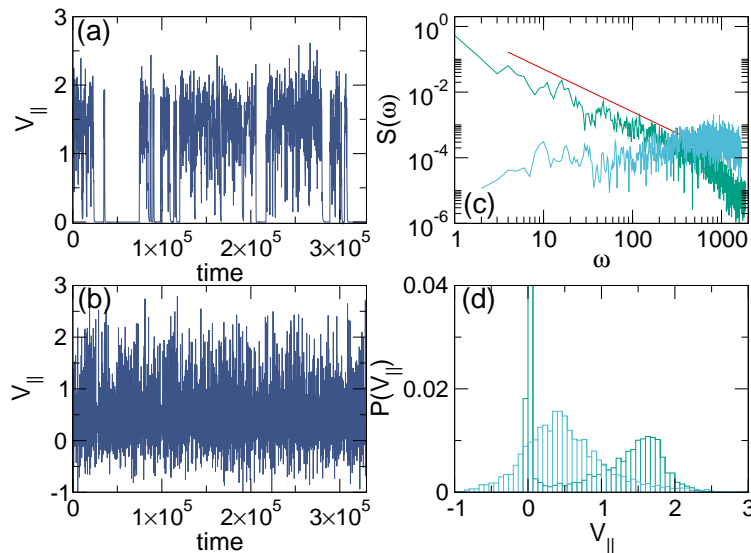


**Figure 9.** Samples with  $n_s = 0.5$ ,  $n_p = 0.3$ ,  $F_p = 2.0$ , and  $F_D = 1.6$ . (a) Time series of  $V_{\parallel}$  for a system with  $\alpha_m/\alpha_d = 0.1$ . (b) Time series of  $V_{\parallel}$  for a system with  $\alpha_m/\alpha_d = 9.95$ . (c) The power spectra  $S(\omega)$  for the  $\alpha_m/\alpha_d = 0.1$  system (green) showing a power law fit to  $1/f^\alpha$  with  $\alpha = 1.3$  (red line), and  $S(\omega)$  for the  $\alpha_m/\alpha_d = 9.95$  system (blue). (d) Distribution  $P(V_{\parallel})$  of velocities in the direction parallel to the drive for the  $\alpha_m/\alpha_d = 0.1$  system (green), where a bimodal shape appears, and for the  $\alpha_m/\alpha_d = 9.95$  system (blue), where the distribution is unimodal.

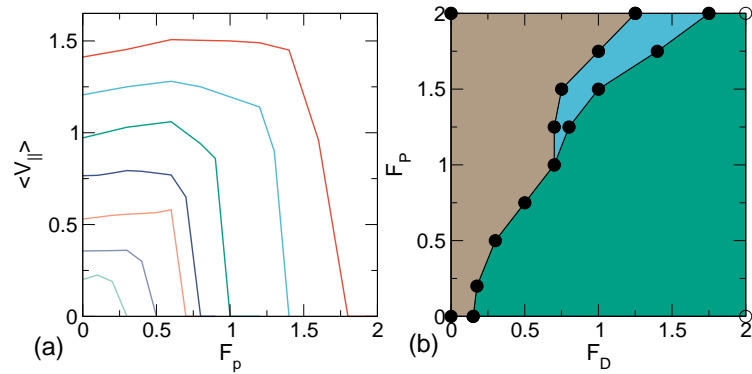


**Figure 10.** (a)  $\langle V_{||} \rangle$  versus pinning strength  $F_p$  for the system in Fig. 9(a) with  $n_s = 0.5$ ,  $n_p = 0.3$ , and  $\alpha_m/\alpha_d = 0.1$  at  $F_D = 2.0, 1.75, 1.5, 1.25, 1.0, 0.7$ , and  $0.5$ , from top to bottom. (b) Dynamic phase diagram for the same system as a function of  $F_p$  versus  $F_D$ . Green: continuous flow regime; blue: stick-slip motion; brown: pinned.

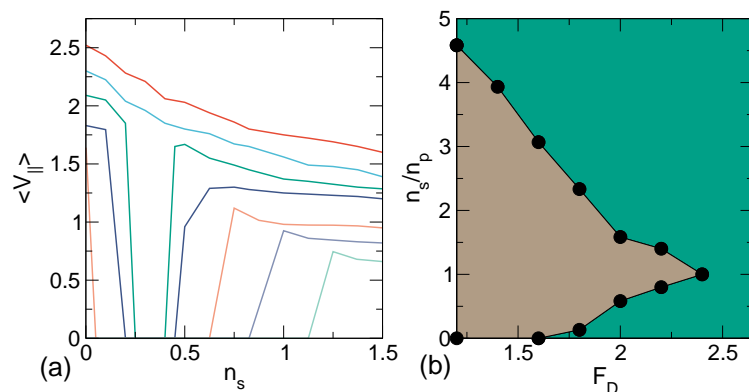


**Figure 11.** (a)  $\langle V_{||} \rangle$  versus skyrmion density  $n_s$  for the system in Fig. 9(a) with  $n_p = 0.3$ ,  $F_p = 1.6$ , and  $\alpha_m/\alpha_d = 0.1$  at  $F_D = 1.4, 1.6, 1.8, 2.0, 2.2, 2.4$ , and  $2.6$ , from bottom to top. (b) Dynamic phase diagram for the same system as a function of  $n_s/n_p$  versus  $F_D$ . Green: continuous flow regime; brown: pinned.

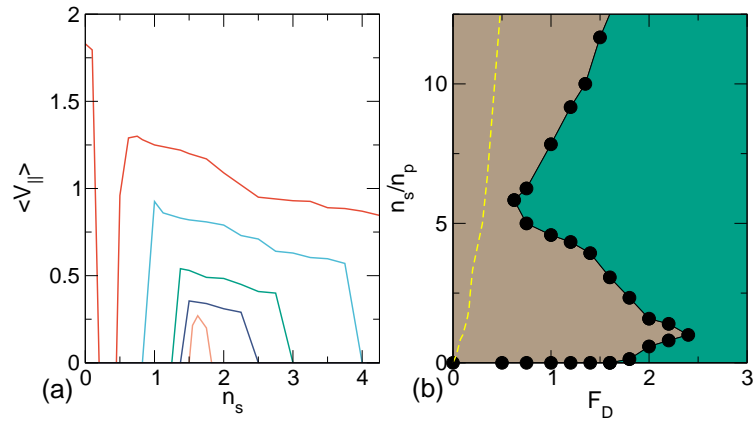


**Figure 12.** (a)  $\langle V_{||} \rangle$  versus  $n_s$  for the system in Fig. 11(a) with  $n_p = 0.3$ ,  $F_p = 1.6$ , and  $\alpha_m/\alpha_d = 0.1$  plotted up to a maximum value of  $n_s = 4.0$  for  $F_D = 0.5, 0.75, 1.0, 1.2, 1.4$ , and  $1.6$ , from bottom to top. (b) Dynamic phase diagram for the same system as a function of  $n_s/n_p$  versus  $F_D$ . Green: continuous flow regime; brown: pinned. The yellow dashed line indicates the location of the depinning threshold in systems with no quenched disorder.